Liquid Crystals
Publication details, including instructions for authors and subscription information:
http://www.informaworld.com/smpp/title~content=t713926090

The effect of substituent position on the liquid crystalline properties of dodecyl-D-xylitols

John W. Goodby; Julie A. Haley; Marcus J. Watson; Grahame Mackenzie; Stephen M. Kelly; Philippe Letellier

Online publication date: 06 August 2010

To cite this Article Goodby, John W. , Haley, Julie A. , Watson, Marcus J. , Mackenzie, Grahame , Kelly, Stephen M. and Letellier, Philippe(1997) 'The effect of substituent position on the liquid crystalline properties of dodecyl-D-xylitols', Liquid Crystals, 22: 4, 497 — 508
To link to this Article: DOI: 10.1080/026782997209225
URL: http://dx.doi.org/10.1080/026782997209225

LIQUID CRYSTALS, 1997, VOL. 22, NO. 4, 497–508

The effect of substituent position on the liquid crystalline properties of dodecyl-D-xylitols

by JOHN W. GOODBY*, JULIE A. HALEY, MARCUS J. WATSON, GRAHAME MACKENZIE, STEPHEN M. KELLY and PHILIPPE LETELLIER

The School of Chemistry, The University of Hull, Hull HU6 7RX, England

PAUL GODE, GERARD GOETHALS, GINO RONCO, BENALI HARMOUCH, PATRICK MARTIN and PIERRE VILLA

Université de Picardie, Jules Verne, Faculté des Sciences, Laboratoire de Chimie Organique et Cinétique, 33 rue Saint Leu, 80039 Amiens, CEDEX, France

(*Received 17 October 1996; accepted 4 November 1996*)

Recently we have been concerned with a systematic and fundamental investigation into the effects of the linking group on the lyotropic and thermotropic properties of aliphatic substituted acyclic carbohydrate systems. For this purpose, we chose to study the self-assembling behaviour of alkyl substituted xylitols where the aliphatic chain was attached to the xylitol moiety *via* ether, ester and thioether linkages. We have extended this work and, in this current study, we report the effects on the self-assembling properties of sequentially moving the position of a dodecyl chain in acyclic x-*O*-dodecyl-D-xylitols. This work was used for a direct comparison with results reported on cyclic systems such as the dodecyl x-*O*-*β*-D-glucopyranosides.

1. Introduction

Alkyl substituted glucopyranosides were recognised as possessing liquid crystalline properties by Noller and Rockwell as long ago as 1938 [1]. Subsequently, the structures of the thermotropic mesophases exhibited by the 1-alkyl *α*-D-glucopyranosides and the 1-alkyl *β*-D-glucopyranosides were investigated by Barrall *et al.* [2], Jeffrey *et al.* [3] and Goodby [4]. The liquid crystalline phase was found, by a variety of techniques, to have a lamellar structure where the amphiphilic molecules have no in-plane or out-of-plane periodic order. Internal phase separation of the aliphatic portions of the molecules and the polar carbohydrate moieties was suggested to give a bilayer structure where either the carbohydrate head groups [4] or the aliphatic chains were interdigitated [5]. Figure 1 shows the preferred structure of the phase where the aliphatic chains are interdigitated and the carbohydrate moieties are organized in disordered layers. This structuring, in conjunction with the molecules being chiral, classifies the phases as smectic A_d^* in type [4]. The structure of the smectic A_d^* mesophase of glycolipids is unusual in that the bilayer structure is inverted with respect to the conventional picture, i.e. it is usually the more rigid parts of the molecules that overlap which in this case would be the sugar units.

In classical non-carbohydrate thermotropic liquid crystal systems, it is common to develop property/structure correlations *via* systematic variation of the molecular structure and comparison of the ensuing transition temperatures. Typically, it is found that the clearing and liquid crystal to liquid crystal transition temperatures are extremely sensitive to structural changes at the molecular level and, in fact, many investigations have been made in relation to the effects of substituent size and position [6]. This is generally not the case with amphitropic systems where neither the thermotropic nor the lyotropic behaviours have been assessed in relation to systematic changes in molecular structure. One such comparison has been completed for dodecyl x-*O*-*β*-D-glucopyranosides by Miethchen *et al.* [7] via the collection of data from previously published results [8, 9]. Figure 2 reproduces the data from Miethchen *et al.* and shows the effect on clearing point temperature as a dodecyl chain is moved sequentially from one position to the next in substituted D-glucopyranose systems.

Recently we have been concerned with a systematic

* Author for correspondence.

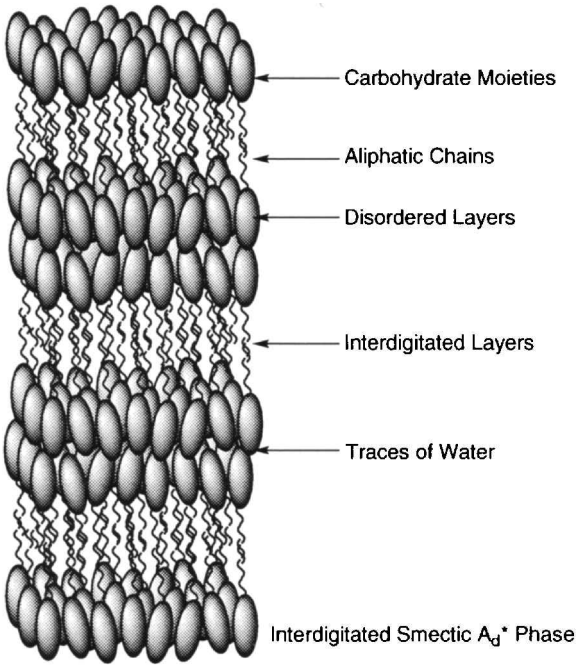

Figure 1. Structure of the smectic A* phase formed by glycolipids.

and fundamental investigation into the effects of the linking group (positioned between the sugar unit and the aliphatic chain in mono-substituted systems) on the lyotropic and thermotropic properties of acyclic systems [10]. For this purpose, we chose to study the self-assembling behaviour of alkyl substituted xylitols where the aliphatic chain was attached to the xylitol moiety *via* ether, ester and thioether linkages, see structure **I** in figure 3. From this investigation, we were able to show that the efficiency for forming thermotropic phases followed the pattern,

$$-SR > -OCOR > -OR$$

whereas, surprisingly, the reverse sequence appeared to be the case for lyotropic phases.

In this current study we report the effects on the self-assembling properties of moving the position of a dodecyl chain in acyclic x-*O*-dodecyl-(D or L)-xylitols—see the family of structures **II** in figure 3. This work can be used as a direct comparison with results reported on cyclic systems by Miethchen *et al.* [7].

2. Experimental procedures

2.1. *General synthetic methods*

The x-*O*-dodecyl-D-xylitols where the dodecyl substituent is linked to a xylitol moiety at the x position (x=1(5), 2, 3 or 4) by an oxygen atom were synthesized according to the scheme. All of the final xylitol products (**15**–**18**) were prepared by regiospecific and stereospecific functionalization of D-xylose.

The 5-D-substituted product, **15**, was prepared *via* derivatization of the anhydro derivative of D-xylose [11], **1**, using dodecan-1-ol in toluene/dimethylsulphoxide to give 5-*O*-dodecyl-1,2- *O*-isopropylidene-α-D-xylofu-

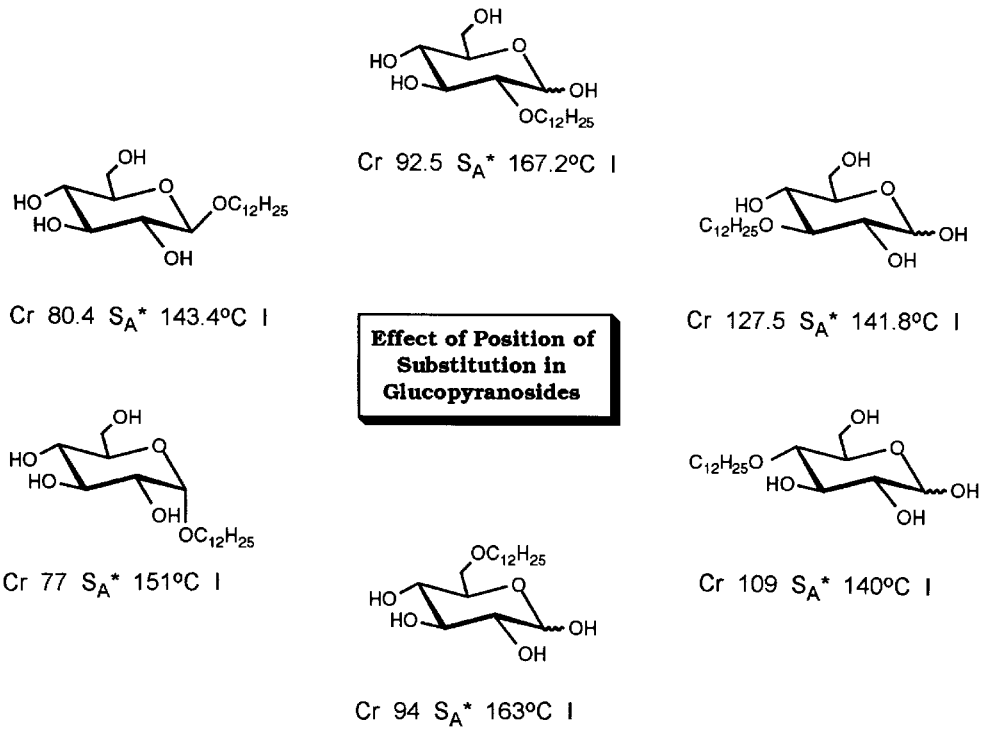

Figure 2. Effect of position of substitution in dodecyl x-*O*-β-D-glucopyranosides.

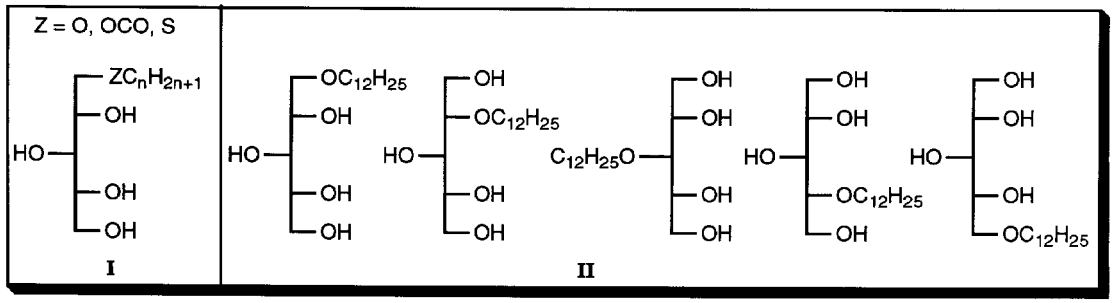

Figure 3. Structures of materials reported in ref. [10] (**I**) and in this work (**II**).

ranose, **2**. Treatment of **2** with sulphuric acid (0·3M) in a mixture of dioxane and water yielded 5-*O*-dodecyl-D-xylofuranose, **3**. Compound **3** was subjected to reduction using sodium borohydride and protonation with cationic resin H^+ to give the final product, **15**.

The 2-substituted product, **16**, was prepared *via* derivatization of the monoacetal of D-xylose [12], **4**, using dodecyl bromide in toluene/dimethylsulphoxide and potassium hydroxide as base to yield methyl 2-*O*-dodecyl-3,5- *O*-isopropylidene-D-xylofuranoside, **5**. Subsequently **5** was deprotected with aqueous acetic acid at 100°C to give 2-*O*-dodecyl-D-xylopyranose, **6**. In a similar way to compound **3**, compound **6** was reduced using sodium borohydride and protonated with cationic resin H^+ to give 2-*O*-dodecyl-D-xylitol, **16**.

The 3-substituted product, **17**, was prepared from the trityl monoacetal, **7**, of D-xylose [13] by the same synthetic procedure as for the preparation of **5** to give compound **8**, 5-*O*-trityl-3-*O*-dodecyl-1,2- *O*-isopropylidene-α-D-xylofuranose. Compound **8** was deprotected using a similar procedure to that for the preparation of compound **3** to give 3-*O*-dodecyl-D-xylopyranose, **9**. In a similar way to compound **3**, compound **9** was reduced with sodium borohydride and protonated with cationic resin H^+ to give 3-*O*-dodecyl-*meso*-xylitol, **17**.

The 4-substituted product, **18**, was prepared in a six step synthetic procedure starting from D-xylose. D-Xylose was first treated with acetyl chloride and allyl alcohol to give allyl α-D-xylopyranoside, **10**. The product was then protected using methoxypropene and a trace of toluene sulphonic acid in DMF to give compound **11**. Allyl 2,3-*O*-isopropylidene-α-D-xylopyranoside, **11**, was derivatized using dodecyl bromide with potassium hydroxide as the base to give the dodecyl product, **12**. Treatment of **12** with potassium *tert*-butoxide in toluene/dimethylsulphoxide gave propenyl 4-*O*-dodecyl-2,3- *O*-isopropylidene-α-D-xylopyranoside, **13**, which was subsequently deprotected to yield **14** and reduced with sodium borohydride and protonated with cationic resin H^+ to give the final product 4-*O*-dodecyl-D-xylitol, **18**.

2.2. *Synthesis of precursor 5-O-dodecyl-D-xylofuranose* (**3**)

2.2.1. *5-O-Dodecyl-1,2-O-isopropylidene-α-D-xylofuranose* (**2**)

Finely powdered potassium hydroxide (6 equiv) and the anhydro derivative **1** [1] (1 equiv) were added to a stirred solution of the dodecan-1-ol (3 equiv) in 1:1 toluene/Me_2SO, at 80°C. After 95% conversion, the mixture was filtered and the filtrate neutralized with saturated aq NH_4Cl. The organic phase was separated, washed with water (twice), dried (Na_2SO_4), and evaporated under reduced pressure. The desired product was isolated after purification by column chromatography. Yield 73·5%, m.p. 62–64°C, $[\alpha]_D^{20} = 0{\cdot}8°$ (c 1·1, $CHCl_3$).

2.2.2. *5-O-Dodecyl-D-xylofuranose* (**3**)

5-*O*-dodecyl-1,2- *O*-isopropylidene-α-D-xylofuranose **2** (100 g l^{-1}) was added at 50°C to a stirred solution of H_2SO_4 (0·3M) in 4:1 dioxane/H_2O. After a 97% conversion, the solution was cooled and neutralized with saturated aq NaOH and solid $NaHCO_3$. The filtrate was evaporated to dryness under reduced pressure, and the desired product was isolated after purification by column chromatography. Yield 63%, m.p. 41–45°C, $[\alpha]_D^{20} = 12{\cdot}9°$ (c 1·0, CH_3OH), $\alpha/\beta = 2/3$ (NMR ^{13}C in C_5D_5N).

2.3. *Synthesis of precursor 2-O-dodecyl-D-xylopyranose* (**6**)

2.3.1. *Methyl 2-O-dodecyl-3,5-O-isopropylidene-D-xylofuranoside* (**5**)

Finely powdered potassium hydroxide (2·4 equiv) and dodecyl bromide (1·1 equiv) were added to a stirred solution of monoacetal **4** [2] (1 equiv) in 4:1 toluene/Me_2SO, at room temperature. After 95% conversion, the mixture was filtered and the filtrate neutralized with saturated aq NH_4Cl. The organic phase was separated, washed with water (twice), dried (Na_2SO_4), and evaporated to dryness under reduced pressure. The desired product was isolated as an oil after purification

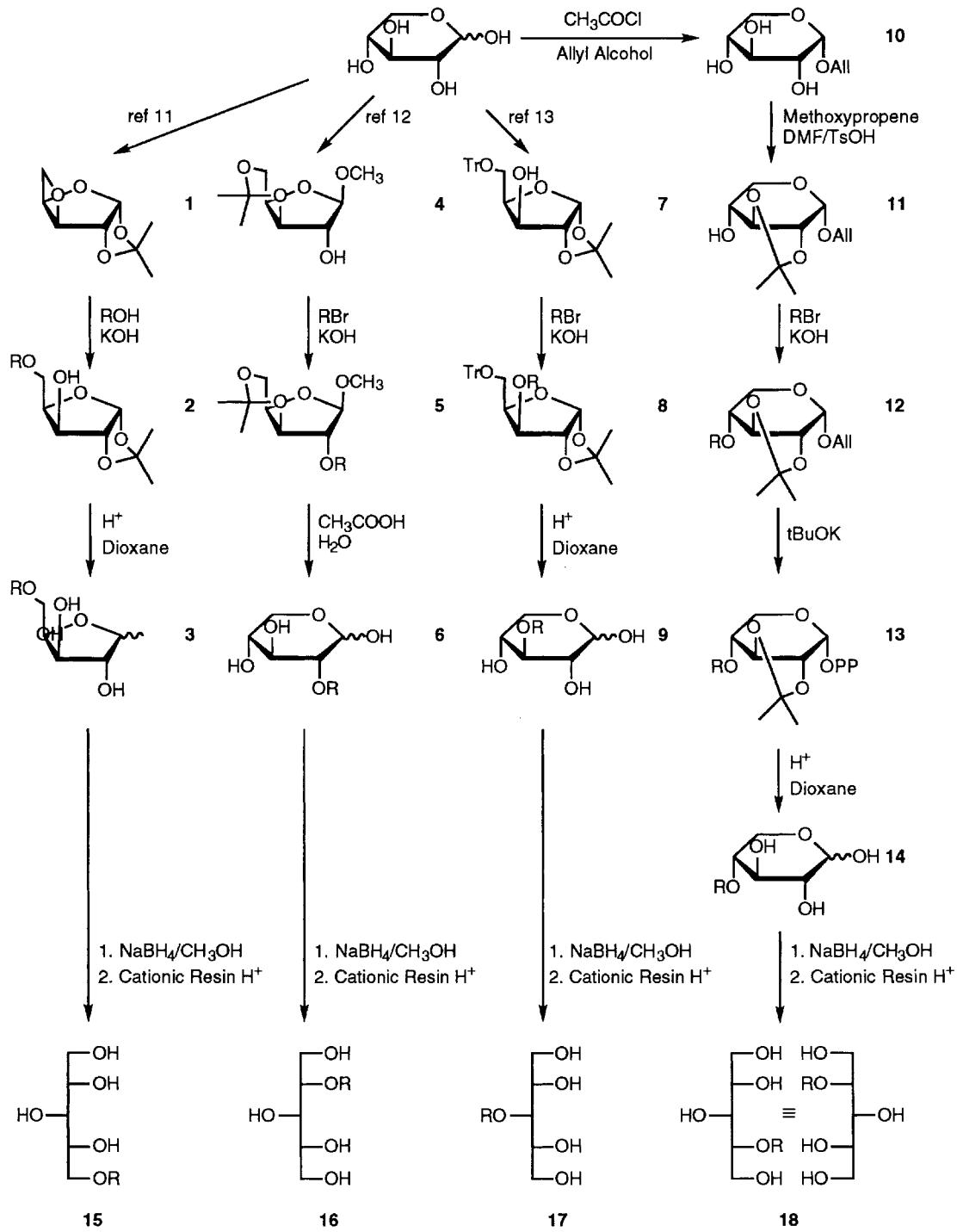

Scheme : Synthesis of Materials, $R = C_{12}H_{25}$

by column chromatography. Yield 80%, $[\alpha]_D^{20} = -44{\cdot}9°$ (c 1·1, $CHCl_3$).

2.3.2. *2-O-Dodecyl-D-xylopyranose* (**6**)

Methyl 2-*O*-dodecyl-3,5- *O*-isopropylidene-D-xylofuranoside **5** (100 g l^{-1}) was added to a stirred solution of 4:1 H_2O/CH_3COOH. After a 97% conversion at 100°C, the solution was evaporated to dryness under reduced pressure. The desired product was isolated after purification by column chromatography. Yield 56%, m.p. 78–81°C, $[\alpha]_D^{20} = 21{\cdot}9°$ (c 1·3, CH_3OH), $\alpha/\beta = 45/55$ (NMR ^{13}C in C_5D_5N).

2.4. *Synthesis of precursor 3-O-dodecyl-D-xylopyranose* (**9**)

2.4.1. *5-O-Trityl-3-O-dodecyl-1,2-O-isopropylidene-α-D-xylofuranose* (**8**)

This material was prepared from the trityl monoacetal **7** [3] using the same method as for the synthesis of compound **5**. Yield 83%, m.p. 58–70°C, $[\alpha]_D^{20} = -25{\cdot}9°$ (c 1·2, $CHCl_3$).

2.4.2. *3-O-Dodecyl-D-xylopyranose* (**9**)

This material was prepared from the monoacetal **8** using the same method as for the synthesis of compound **3**, but in this case with the temperature at solvent reflux instead of 50°C. Yield 70%, m.p. 95–115°C, $[\alpha]_D^{20} = 13{\cdot}5°$ (c 1·5, CH_3OH), $\alpha/\beta = 44/56$ (NMR ^{13}C in C_5D_5N).

2.5. *Synthesis of precursor 4-O-dodecyl-D-xylopyranose* (**14**)

2.5.1. *Allyl α-D-xylopyranoside* (**10**)

Acetyl chloride (50 ml, 2 equiv) and D-xylopyranose (50 g, 1 equiv) were added with stirring to allyl alcohol (200 ml, 9 equiv), at 0°C. After 95% conversion, at room temperature, the mixture was cooled and neutralized with solid $NaHCO_3$. The solution was filtered (Celite) with the aid of 4:1 diethyl ether/THF, and the resulting filtrate evaporated under reduced pressure. Allyl α-D-xylopyranoside **10** was isolated after purification by column chromatography. Yield 55%, m.p. 106–109°C, $[\alpha]_D^{20} = 159{\cdot}5°$ (c 1·0, CH_3OH).

2.5.2. *Allyl 2,3-O-isopropylidene-α-D-xylopyranoside* (**11**)

Methoxypropene (1·2 equiv) and TsOH (trace) were added to a stirred solution of allyl α-D-xylopyranoside **10** (1 equiv) in DMF (100 g l^{-1}) at 0°C. After the reaction was complete at room temperature (97% conversion), the solution was cooled and neutralized with solid $NaHCO_3$. The filtrate was evaporated under reduced pressure, and allyl 2,3-*O*-isopropylidene-α-D-xylopyranoside **11** was isolated after purification by column chromatography. Yield 70%, m.p. 74–76°C, $[\alpha]_D^{20} = 146{\cdot}6°$ (c 1·1, $CHCl_3$).

2.5.3. *Allyl 4-O-dodecyl-2,3-O-isopropylidene-α-D-xylopyranoside* (**12**)

This material was prepared from the monoacetal **11** using the same method as for the synthesis of compound **5**. Yield 76%, m.p. 29–31°C, $[\alpha]_D^{20} = 93{\cdot}7°$ (c 1·0, $CHCl_3$).

2.5.4. *Propenyl 4-O-dodecyl-2,3-O-isopropylidene-α-D-xylopyranoside* (**13**)

Potassium *tert*-butoxide (2 equiv) was added to a stirred solution of allyl 4-*O*-alkyl-2,3-*O*-isopropylidene-D-xylopyranoside **12** in 1:1 toluene/Me_2SO (100 g l^{-1}). After the reaction was complete at 100°C (97% conversion), the mixture was filtered and the filtrate neutralized with saturated aq NH_4Cl. The organic phase was separated, washed with water (twice), dried (Na_2SO_4), and evaporated under reduced pressure. The desired product was isolated as an oil after purification by column chromatography. Yield 86%, $[\alpha]_D^{20} = 59{\cdot}8°$ (c 1·1, $CHCl_3$).

2.5.5. *4-O-Dodecyl-D-xylopyranose* (**14**)

Propenyl 4-*O*-alkyl-2,3-*O*-isopropylidene-α-D-xylopyranoside **13** (100 g l^{-1}) was added to a stirred solution of H_2SO_4 (0·2M) in 4:1 dioxane/H_2O. After the reaction was complete at 50°C (97% conversion), the solution was cooled and neutralized with saturated aq NaOH and solid $NaHCO_3$. The filtrate was evaporated under reduced pressure, and 4-*O*-dodecyl-D-xylopyranose **14** was isolated after purification by column chromatography. Yield 70%, m.p. 90–125°C, $[\alpha]_D^{20} = 25{\cdot}6°$ (c 1·2, CH_3OH), $\alpha/\beta = 7/3$ (NMR ^{13}C in C_5D_5N).

2.6. *General method for the reduction of the x-O-dodecyl-D-xyloses to alditols* **15** *to* **18**

Each xylose derivative, **3**, **6**, **9**, **14**, (50 g l^{-1}) was dissolved in methanol and treated with sodium borohydride (6 equiv) at room temperature for 16 h. The sodium borohydride excess was destroyed by treatment with formic acid for 5 h at room temperature and the solution was concentrated under reduced pressure. Cationic resin H^+ was added to a solution of the crude products in 1:1 MeOH/H_2O. After 15 min the mixture was filtered and the filtrate was evaporated under reduced pressure. The desired products were isolated and purified by column chromatography with a mixture of hexane/THF (1:9).

2.6.1. *5-O-Dodecyl-D-xylitol* (**15**)

Yield 2·8 g, 56%, $[\alpha]_D^{20} = 1{\cdot}2°$ (c 1·0, CH_3OH). ^1H NMR (300 MHz, C_5D_5N) δ: 0·84 (t, $J_{\omega\omega-1} = 6{\cdot}4$ Hz, 3H, Hω); 1·20 (m, $(CH_2)_9$); 1·56 (m, $J_{\alpha\beta} = 6{\cdot}6$ Hz, 2H, Hβ); 3·48 (t, 2H, Hα); 3·94 (dd, $J_{4,5b} = 6{\cdot}3$ Hz, 1H, H-5b); 4·02 (dd, $J_{4,5a} = 5{\cdot}2$ Hz, $J_{5a,5b} = 10{\cdot}2$ Hz, 1H, H-5a); 4·26 (dd, $J_{1b,2} = 5{\cdot}8$ Hz, 1H, H-1b); 4·31 (dd, $J_{1a,2} = 5{\cdot}2$ Hz, $J_{1a,1b} = 10{\cdot}9$ Hz, 1H, H-1a); 4·37 (dd, $J_{3,4} = 3{\cdot}5$ Hz, 1H, H-3); 4·48 (m, $J_{2,3} = 3{\cdot}5$ Hz, 1H, H-2); 4·55 (m, m 1H, H-4). ^{13}C NMR (75 MHz, C_5D_5N) δ: 14·6 (Cω); 23·2–32·4 $(CH_2)_9$; 30·5 (Cβ); 64·8 (C-1); 72·0 (Cα); 72·5 (C-3); 72·6 (C-4); 73·9 (C-5; 74·7 (C-2). Elemental analysis: calcd for $C_{17}H_{36}O_5$: C 63·71, H 11·32; found: C 63·51, H 11·21.

2.6.2. *2-O-Dodecyl-D-xylitol* (**16**)

Yield 1·1 g, 57%, $[\alpha]_D^{20} = 3{\cdot}2°$ (c 1·1, CH_3OH). ^1H NMR (300 MHz, C_5D_5N) δ: 0·85 (t, $J_{\omega\omega-1} = 6{\cdot}7$ Hz, 3H, Hω); 1·19 (m, $(CH_2)_9$); 1·61 (m, $J_{\alpha\beta} = 6{\cdot}7$ Hz, 2H, Hβ); 3·72 (dt, $J_{\alpha\alpha'} = 9{\cdot}1$ Hz, 1H, H-α'); 3·88 (dt, 1H, H-α); 4·09 (ddd, $J_{2,3} = 4{\cdot}6$ Hz, $J_{1a,2} = 4{\cdot}6$ Hz, 1H, H-2); 4·29 (dd,

$J_{5a,5b}=10{\cdot}7$ Hz, $J_{4,5b}=6{\cdot}0$ Hz, 1H, H-5b); 4·32 (dd, $J_{1a,1b}=11{\cdot}3$ Hz, $J_{1b,2}=4{\cdot}5$ Hz, 1H, H-1b); 4·36 (dd, $J_{4,5a}=5{\cdot}0$ Hz, 1H, H-5a); 4·42 (dd, 1H, H-1a); 4·57 (ddd, $J_{3,4}=3{\cdot}5$ Hz, 1H, H-4); 4·60 (dd, 1H, H-3). ^{13}C NMR (75 MHz, C_5D_5N) δ: 14·6 (Cω); 23·3–31·1 (CH_2)$_9$; 31·1 (Cβ); 61·9 (C-1); 65·2 (C-5); 71·4 (Cα); 72·4 (C-3); 73·2 (C-4); 83·2 (C-2). Elemental analysis: calcd for $C_{17}H_{36}O_5$: C 63·71, H 11·32; found: C 64·03, H 11·34.

2.6.3. *3-O-Dodecyl-meso-xylitol* (**17**)

Yield 3·4 g, 53%. ^{1}H NMR (300 MHz, C_5D_5N) δ: 0·84 (t, $J_{\omega\omega-1}=6{\cdot}7$ Hz, 3H, Hω); 1·19 (m, (CH_2)$_9$); 1·61 (m, $J_{\alpha\beta}=6{\cdot}5$ Hz, 2H, Hβ); 3·93 (t, 2H, Hα); 4·18 (dd, $J_{2,3}=J_{3,4}=3{\cdot}8$ Hz 1H, H-3, 4·30–4·34 (m, 4H, H-1, and H-5); 4·62 (m, $J_{1,2}=J_{4,5}=5{\cdot}4$ Hz, 2H, H-2 and H-4). ^{13}C NMR (75 MHz, C_5D_5N) δ: 14·6 (Cω); 23·3–32·4 (CH_2)$_9$; 31·3 (Cβ); 64·6 (C-1 and C-5); 73·3 (Cα); 73·6 (C-2 and C-4); 81·5 (C-3). Elemental analysis: calcd for $C_{17}H_{36}O_5$: C 63·75, H 11·25; found: C 63·57, H 11·33.

2.6.4. *4-O-Dodecyl-D-xylitol* (**18**)

Yield 0·5 g, 55%, $[\alpha]_D^{20}=-1{\cdot}2°$ (c 1·0, CH_3OH). ^{1}H NMR (300 MHz, C_5D_5N) δ: 0·81 (t, $J_{\omega\omega-1}=6{\cdot}6$ Hz, 3H, Hω); 1·17 (m, (CH_2)$_9$); 1·57 (m, $J_{\alpha\beta}=6{\cdot}7$ Hz, 2H, Hβ); 3·68 (dt, $J_{\alpha\alpha'}=9{\cdot}1$ Hz, 1H, Hα); 3·84 (dt, 1H, Hα); 4·03 (ddd, $J_{4,5b}=4{\cdot}6$ Hz, 1H, H-4); 4·23 (dd, $J_{1b,2}=5{\cdot}9$ Hz, H-1b); 4·29 (dd, $J_{4,5b}=4{\cdot}6$ Hz, $J_{5a,5b}=11{\cdot}5$ Hz, 1H, H-5b); 4·31 (dd, $J_{1a,1b}=10{\cdot}6$ Hz, $J_{1a,2}=5{\cdot}0$ Hz, 1H, H-1a); 4·36 (dd, $J_{4,5a}=4{\cdot}5$ Hz, 1H, H-5a); 4·51 (ddd, $J_{2,3}=3{\cdot}4$ Hz, 1H, H-2); 4·53 (tdd $J_{3,4}=4{\cdot}6$ Hz, 1H, H-3). ^{13}C NMR (75 MHz, C_5D_5N) δ: 14·7 (Cω); 23·3–32·5 ((CH_2)$_9$); 31·1 (Cβ); 61·9 (C-5); 65·2 (C-1); 72·4 (C-3); 73·1 (C-2); 83·3 (C-4). Elemental analysis: calcd for $C_{17}H_{36}O_5$: C 63·71, H 11·32; found: C 63·60, H 11·30.

2.7. *Characterisation of materials and measurement of physical properties*

All of the chemical reactions were monitored by either reverse phase HPLC (Waters 721) or GPC (Girdel) chromatography. Reverse phase HPLC was carried out using either RP-18 (Merck) or PN 27-196 (Waters) columns, whereas GPC was performed using either OV 17 or SE 30 columns. Purification of the final products was achieved by gradient column chromatography over silica gel (60 mesh, Matrex) using a mixture of hexane/acetone as the eluent (in each case the ratio of silica gel to product mixture to be purified was 30:1). The purities of the final compounds were determined by chromatographic, spectroscopic, and elemental analyses. The structures of all of the materials, intermediates and final products, were determined by a combination of spectroscopic methods, for example, NMR spectra were recorded using a Bruker WB-300 spectrometer for solutions in $CDCl_3$ or C_5D_5N (tetramethylsilane was used as the internal standard). The melting point of each product was determined using an electrothermal automatic apparatus (the results reported are uncorrected).

Phase identifications and determination of phase transition temperatures were made concomitantly by thermal polarized light microscopy using either a Zeiss Universal or a Leitz Laborlux 12 Pol polarizing transmitted light microscope equipped with a Mettler FP82 microfurnace in conjunction with an FP80 Central Processor. Homeotropic sample preparations suitable for phase characterization were prepared simply by using cleaned glass microscope slides (washed with water, acetone, water, concentrated nitric acid, water and dry acetone), whereas homogeneous defect textures were obtained by using nylon coated slides. Nylon coating of the slides (~200–300 Å thick) was obtained by dipping clean slides into a solution of nylon (6/6) in formic acid (1% wt/vol). The nylon solution was allowed to drain off the slides over a period of 1 h, and then they were baked dry, free from solvent, in an oven at 100°C for a period of 3 h. The slides were not buffed, as is usual for preparing aligned samples, but instead they were used untreated so that many defects would be created when the liquid crystal formed on the surface of the slide on cooling from the liquid phase.

Differential scanning calorimetry was used to determine enthalpies of transition and to confirm the phase transition temperatures determined by optical microscopy. Differential scanning thermograms (scan rate 10° min^{-1}) were obtained using a Perkin Elmer DSC 7 PC system operating on UNIX software. The results obtained were standardized relative to indium (measured onset 156·7°C, ΔH 28·5 J g^{-1}, literature value 156·6°C, ΔH 28·45 J g^{-1}) [14]. Comparison of the transition temperatures determined by optical microscopy and differential scanning calorimetry show some slight discrepancies. This is due to two factors: firstly, the two methods used separate instruments which are calibrated in different ways, and secondly, and more importantly, the carbohydrates tended to decompose slightly at elevated temperatures and at different rates depending on the rate of heating, the time spent at an elevated temperature and the nature of the supporting substrate, i.e. the materials decomposed more quickly in aluminium DSC pans than on glass microscope slides.

Classification of the mesophases of the products was achieved *via* binary phase diagrams which were constructed by determining the phase transition temperatures of individual binary mixtures of a test material mixed with a standard compound of known phase transition sequence. The binary mixtures were produced by weighing out each individual test material and a known standard material on a microscope slide and mixing them thoroughly while in their liquid states. The

cooled samples were introduced into the microscope microfurnace and the phase transition temperatures and classification of phase type were obtained in the usual manner. Typically, when the test and standard materials were mixed on a microscope slide while in their liquid states, some decomposition occurred thereby resulting in lower transition temperatures. In all cases, recrystallization temperatures were not determined because the binary mixtures supercooled to room temperature in their liquid crystalline states.

Molecular modelling studies were performed on a Silicon Graphics workstation (Indigo XS24, 4000) using the programs Quanta and CHARMm. Within CHARMm, the Adopted Basis Newton Raphson (ABNR) algorithm was used to locate the molecular conformation with the lowest potential energy. The minimization calculations were performed until the root mean square (RMS) force reached 4·184 kJ mol^{-1} Å^{-1}, which is close to the resolution limit. The RMS force is a direct measure of the tolerance applied to the energy gradient (i.e. the rate of change of potential energy with step number) during each cycle of minimization. The calculation was terminated in cases where the average energy gradient was less than the specified value. The results of the molecular mechanics calculations were generated using the programs QUANTA V4.0 and CHARMm V22.2. The programs were developed and integrated by Molecular Simulations Inc. The modelling packages assume the molecules to be a collection of hard particles held together by elastic forces, in the gas phase, at absolute zero, in an ideal motionless state, and the force fields used are those described in CHARMm V22.2.

3. Results and discussion

3.1. *Phase classification*

3.1.1. *Transition temperatures and enthalpies*

The clearing points (cl.p) were determined by thermal optical microscopy whereas the melting points (m.p.) and recrystallization (recryst.) temperatures were measured by differential scanning calorimetry. The enthalpies of all of the phase transitions were also evaluated from differential scanning calorimetry. The results obtained from both techniques of study are shown together in the table.

There are some interesting trends that can be deduced from the table. First, as the chain is moved towards the centre of the carbohydrate moiety, the clearing transition temperatures rise almost linearly in relation to the position of the aliphatic chain with respect to the ends of the carbohydrate moiety. Second, the melting points rise as the chain is moved towards the centre of the carbohydrate moiety, but this time the trends, although symmetrical, are not linear from either end of the carbohydrate moiety. Third, the temperature range of the thermotropic mesophase decreases as the chain is moved to the centre. Fourth, the recrystallization temperatures are similar to the other trends, i.e. highest when the chain is positioned at the centre. Figure 4 shows these trends as a function of position of the dodecyl chain (note positions 1 and 5 are equivalent).

Table. Transition temperatures (°C) and enthalpies of transition, ΔH (J g^{-1}) (in square brackets) as a function of position of substitution in the x-*O*-dodecyl-(D)-xylitols.

Compound	Transition temperatures/°C
15	Smectic A* 114·7 Isotropic liquid m.p. 49·5 [113·5] cl.p. 111·1 [3·9] recryst. 19·4 [101·5]
16	Smectic A* 123·1 Isotropic liquid m.p. 69·1 [178·1] cl.p. 120·3 [6·0] recryst. 37·9 [156·4]
17	Smectic A* 138·0 Isotropic liquid m.p. 101·3 [161·1] cl.p. 137·3 [6·95] recryst. 57·9 [143·5]
18	Smectic A* 123·8 Isotropic liquid m.p. 67·8 [139·6] cl.p. 123·7 [5·9] recryst. 28·3 [51·9]

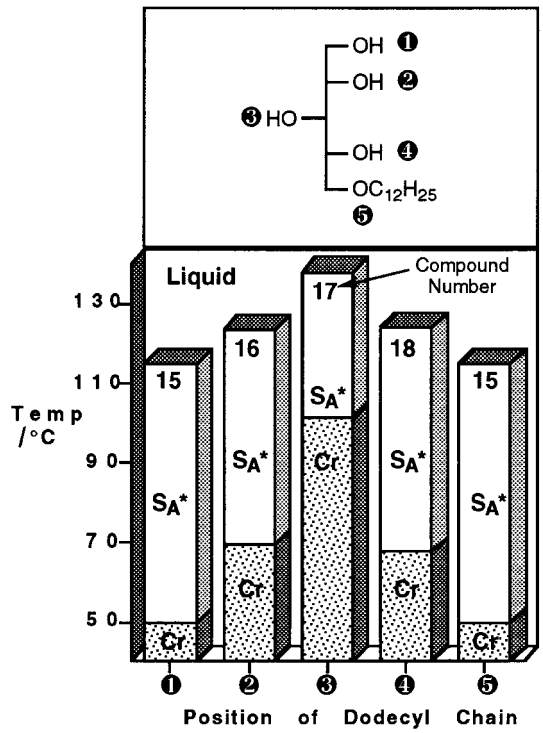

Figure 4. Variation in transition temperatures as a function of position of the aliphatic chain for compounds **15** to **18** inclusive.

The enthalpy and entropy values for the clearing points, like the transition temperatures, rise as the chain is moved towards the centre of the molecule, see figures 5(*a*) and (*b*) respectively. All of these results indicate that the materials become more 'crystalline' in nature as the molecular structure becomes more symmetrical by moving the chain towards the centre of the carbohydrate moiety.

3.1.2. *Phase characterization*

The mesophases exhibited by all of the compounds were determined by co-miscibility within the series to be of the same type. Thus, the materials exhibit a single liquid crystal phase. Classification was achieved in two ways: firstly from observations of the defect textures exhibited by the mesophase on cooling from the isotropic liquid, and secondly through miscibility studies with a standard material.

The defect textures exhibited by the mesophase fall into three categories. On untreated clean glass substrates focal-conic, oily streak and homeotropic defect textures were observed. On glass substrates coated with nylon, homogeneous alignment was achieved, and focal-conic defects characterized by their elliptical and hyperbolic lines of optical discontinuity were observed. The presence of focal-conic defects and homeotropic alignment in variously treated specimens is diagnostic for the presence of a smectic A phase. In addition, as the molecules are chiral, the specimens were examined for any indication of the formation of a helical macrostructure, e.g. banding in the focal-conic domains, rotation of plane polarized light and selective reflection of light; however, none of these effects was found. Thus, the materials do not exhibit the twisted form of the smectic A* phase, i.e. the twist grain boundary phase. These results classify the phase as being smectic A* in type.

Miscibility studies with octyl 1-*O*-β-D-glucopyranoside [4], which is a standardized carbohydrate that exhibits smectic A_d^* phase, confirmed the above classification of the liquid crystal phase.

Thus, the phase exhibited by the materials is found to be smectic A* with a structure expected to resemble that shown in figure 1. In this structure the aliphatic chains in adjacent pairs of layers are expected to interdigitate partially. The carbohydrate moieties, on the other hand, are expected to be arranged on the peripheral surfaces of the bilayer structure, and thus the resulting structure resembles that of a membrane. The mesophase could, therefore, be classified as an interdigitated bilayer structure, and as the stronger intermolecular interactions are at the surfaces of the bilayer ordering, the structure could be said to be inverted relative to that normally found for the smectic A phase where the strong interactions are more likely to be found within the layer [5]. Thus, the proposed structure for the mesophase is in keeping with structures reported for similar phases of carbohydrate liquid crystals, that is as smectic A_d^*.

3.2. *Molecular simulations*

In order to examine the nature (rigidity/flexibility/shape) of the molecular structures of the compounds, each individual material was geometrically optimized. The minimized structures for all of the materials are shown together for comparison in figure 6. It can be seen from figure 6 that the 3-substituted material is indeed the most symmetrical of the five compounds, and in this representation it also appears as the shortest and broadest of the materials, i.e. it might be expected to

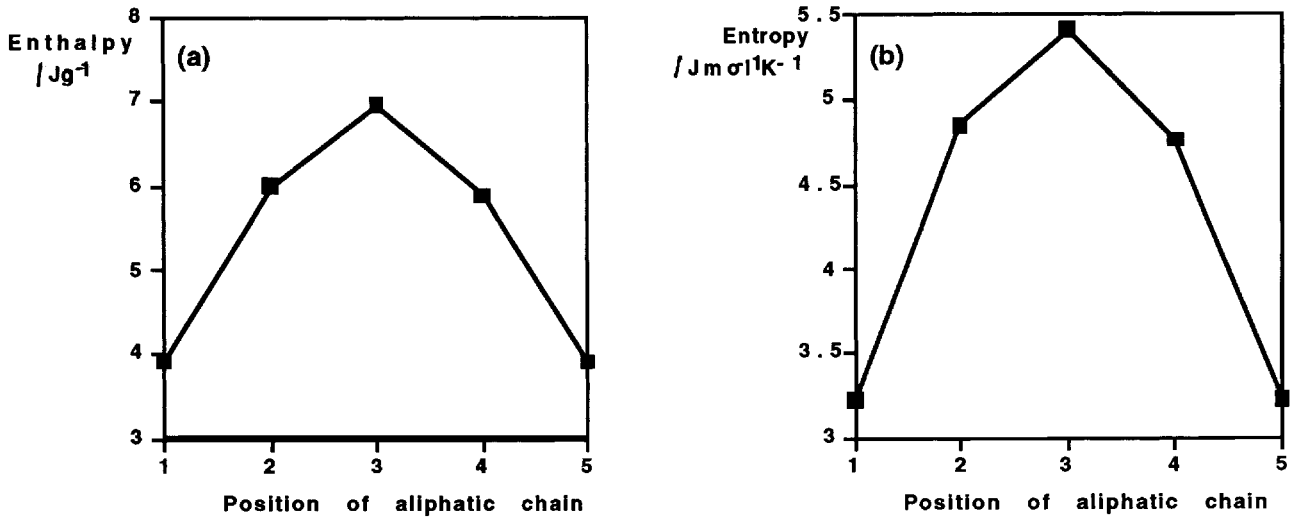

Figure 5. Variation in (*a*) enthalpy ($J\,g^{-1}$) and (*b*) entropy ($J\,mol^{-1}\,K^{-1}$) of the clearing points as a function of position of the aliphatic chain for **15** to **18**; positions 1- and 5- are equivalent.

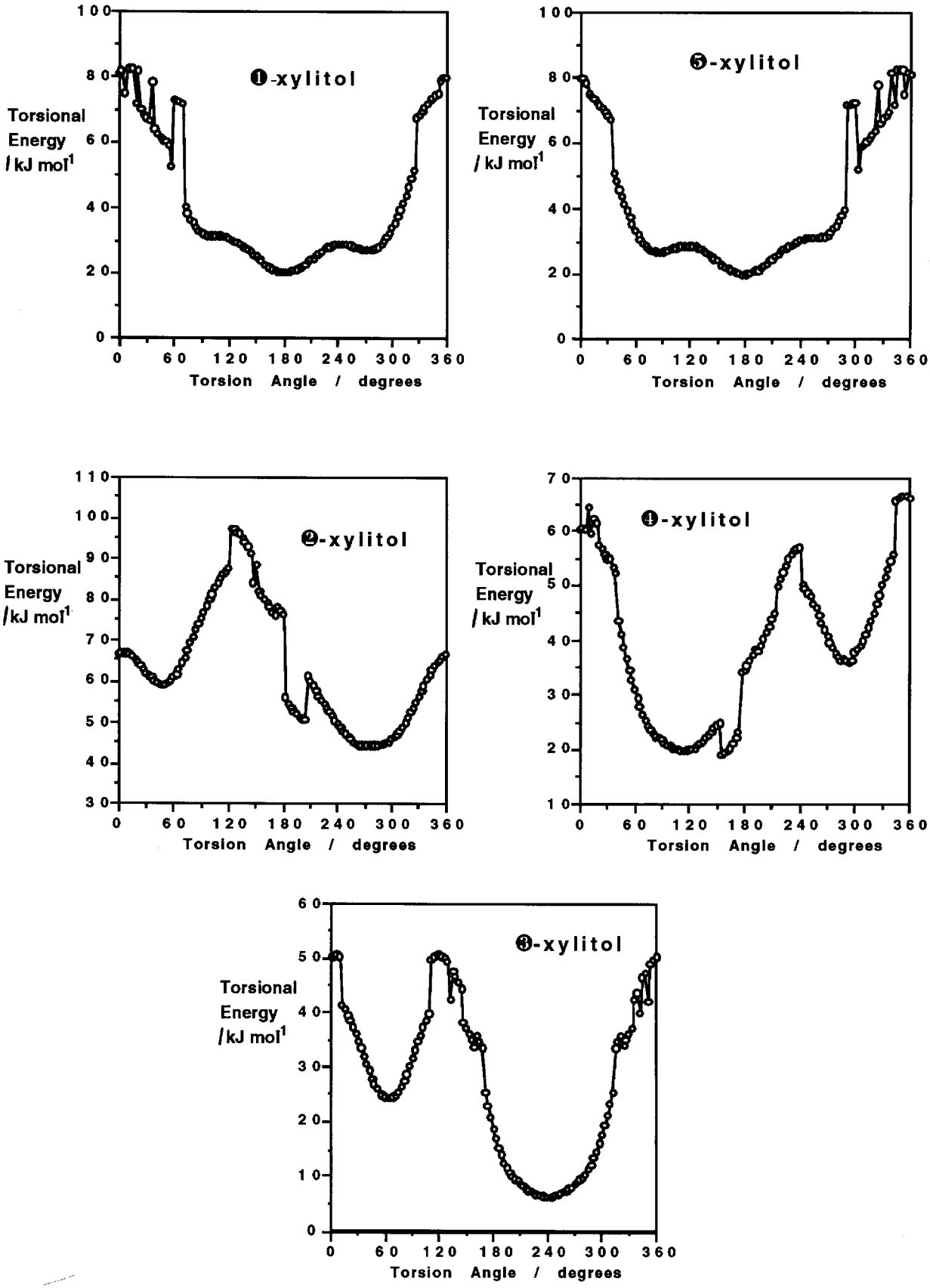

Figure 7. The torsional energy as a function of torsional angle (3° step intervals) for each isomer.

have the least molecular shape anisotropy. Traditional thinking would tend to suggest, at least from the point of view of molecular shape, that a high degree of anisotropy would lead to a high clearing point for compounds 1 and 5, whereas a lower molecular anisotropy would produce a lower clearing point. These views are contradictory for the 3-substituted material; however, it is also expected that the increased stiffness about the carbohydrate moiety could also have an effect on clearing point. The mobility about the carbohydrate to aliphatic chain region of the molecules was investigated in the following simulations.

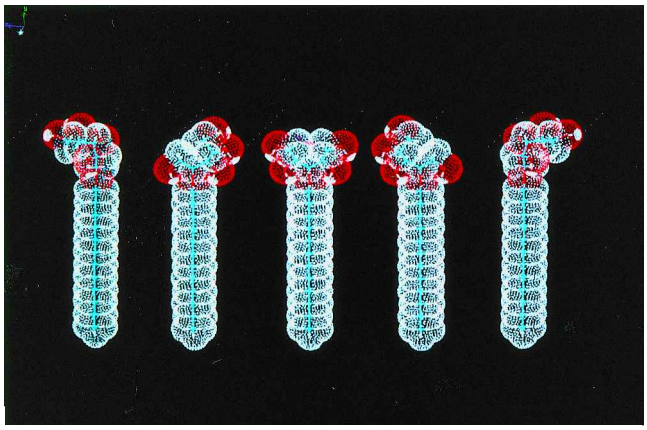

Figure 6.

Simulation of the xylitol derivatives was also carried out at a temperature within the smectic A* phase. CHARMm dynamics were achieved constraining only bonds containing hydrogens and using the parameter-specified geometry. The molecular dynamics calculations were carried out in three stages: heating, equilibrating the molecule and then simulating the motion of the molecule at the following temperatures in the gas phase.

5-substituent – 383 K; 4-substituent – 393 K;
3-substituent – 408 K; 2-substituent – 393 K;
1-substituent – 383 K

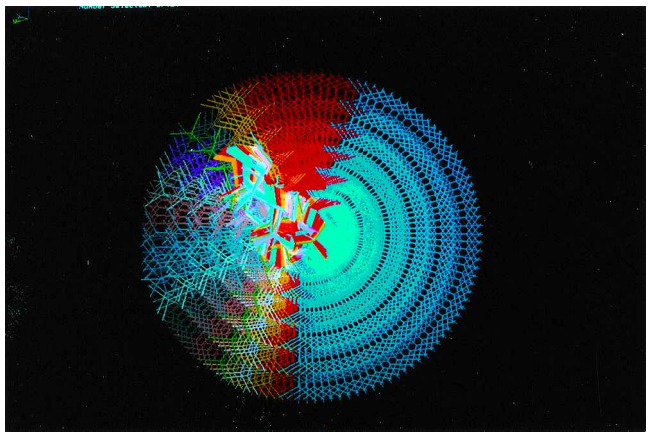

Figure 8.

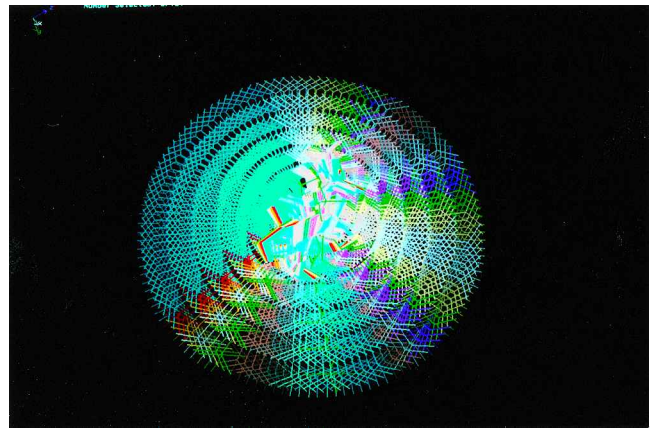

Figure 10.

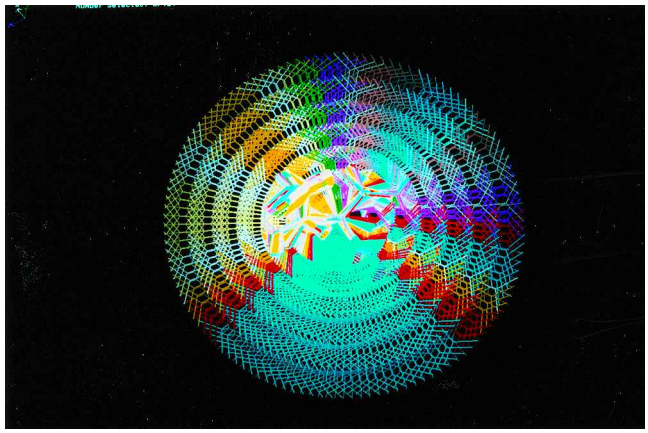

Figure 9.

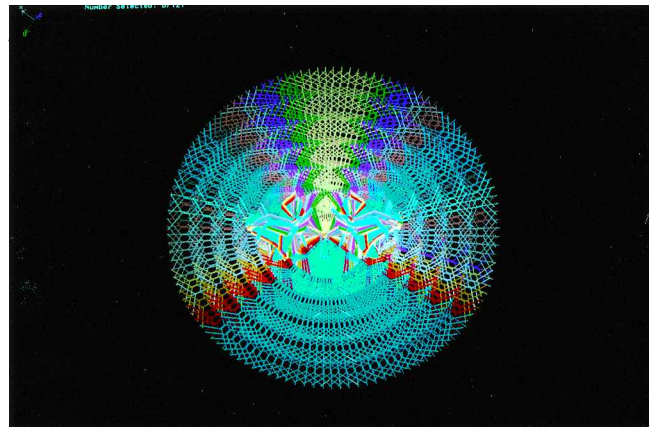

Figure 11.

The first two stages were necessary to prepare the model for the third simulation stage where CHARMm dynamics were performed for a simulated time of 6·4 ps, generating 640 conformations. Average coordinates of these conformations produced time-average structures of the xylitol derivatives which were respectively found to be very similar to the conformations with the lowest potential energy (see figure 6).

The relative mobilities between the core and aliphatic tail of the three xylitol derivatives were studied by allowing the substituent to rotate relative to the carbohydrate core. A conformational search around the O–C bond (carbohydrate to aliphatic chain) was performed on the geometrically optimized structures. The search was done in a systematic way, using a 360° scan of the appropriate torsion angle with a 3° step sequence and, at each step, the grid torsion was defined and artificially fixed to prevent the structure from returning to the original geometrically optimized structure. Each conformation generated in the stepwise rotation was geometrically optimized using a conjugate gradient algorithm and an energy gradient tolerance equal to $4{\cdot}184\,\mathrm{kJ\,mol^{-1}\,\AA^{-1}}$. The torsional energy as a function of torsional angle (3° step intervals) for each isomer is shown in figure 7. It can be seen that the graphs for the 1- and 5-substituted xylitols are mirror images, as are the graphs for the 2- and 4-substituted materials. The depth and the breadth of the minima in the torsional energy describe, to some extent, the freedom of motion of the terminal dodecyl chain relative to the carbohydrate moiety.

The minimized rotational structures were then overlaid in order to generate a pictorial model of the relative positions and energies of the different rotational conformers produced, see figures 8 to 11 (due to symmetry figure 8 = 1- and 5-isomers, figure 9 = 2-isomer, figure 10 = 4-isomer, and figure 11 = 3-isomer). In these figures, the long axis of the xylitol moiety is perpendicular to the plane of the figure, and the freedom of motion of the aliphatic chain is shown as a disc centred on the xylitol unit. The colour coding of the disc depicts the relative degree of freedom of the dodecyl chain. The colour blue depicts a fairly unrestricted chain; at the other extreme white represents a restricted environment for the chain. It can be seen from these figures that the 3-isomer, as predicted, has the most restricted motion about the chain carbohydrate linkage, followed closely by the 2- and 4-isomers. The 1- and 5-isomers, by comparison, have relatively free motion of the aliphatic chain with respect to the carbohydrate moiety. These results mirror those found for the clearing, melting and recrystallization temperatures and for the enthalpy and entropy values.

Overall, we can see that by increasing the symmetry and stiffening the structure of a glycolipid about the junction of the aliphatic chain to the carbohydrate moiety we can increase the clearing point transitions for thermotropic phases. The improved aspects of symmetry across the series of compounds can be seen quite clearly in figure 6. The 3-isomer almost forms a quasi-hexagonal structure about the polar head group (which might indeed be facilitated by intramolecular hydrogen bonding). These improved aspects of symmetry and decrease in mobility of the end chain far outweigh the decrease in molecular anisotropy for the 3-isomer in relation to the other isomers, and thus it has the highest clearing temperature and hence the most stable liquid crystal phase (as demonstrated by the results obtained for the measurements of the enthalpies and entropies of transition).

4. Conclusion

We have demonstrated that there is a relationship between molecular flexibility/rigidity and symmetry/asymmetry in acyclic glycolipid systems that impinges

Figure 6. The minimized energy conformations of the dodecyl isomers (left to right 5-, 4-, 3-, 2-, 1-*O*-dodecyl xylitols).

Figure 8. The stepwise rotations (about a total rotation of 360°) of the alkyl chain of 5- or 1-*O*-dodecyl substituted xylitols about the carbohydrate to aliphatic chain carbon–oxygen bond. The superimposed sugar moieties appear at the centre of the figure, whereas the superimposed rotational conformers of the aliphatic chain appear spread out in a disc. Blue shows regions where the chain has the most freedom to rotate, white shows regions where it is restricted.

Figure 9. The stepwise rotations (about a total rotation of 360°) of the alkyl chain of the 2-*O*-dodecyl substituted xylitol about the carbohydrate to aliphatic chain carbon–oxygen bond. The superimposed sugar moieties appear at the centre of the figure, whereas the superimposed rotational conformers of the aliphatic chain appear spread out in a disc. Blue shows regions where the chain has the most freedom to rotate, white shows regions where it is restricted.

Figure 10. The stepwise rotations (about a total rotation of 360°) of the alkyl chain of the 4-*O*-dodecyl substituted xylitol about the carbohydrate to aliphatic chain carbon-oxygen bond. The superimposed sugar moieties appear at the centre of the figure, whereas the superimposed rotational conformers of the aliphatic chain appear spread out in a disc. Blue shows regions where the chain has the most freedom to rotate, white shows regions where it is restricted.

Figure 11. The stepwise rotations (about a total rotation of 360°) of the alkyl chain of 3-*O*-dodecyl-*meso*-xylitol about the carbohydrate to aliphatic chain carbon–oxygen bond. The superimposed sugar moieties appear at the centre of the figure, whereas the superimposed rotational conformers of the aliphatic chain appear spread out in a disc. Blue shows regions where the chain has the most freedom to rotate, white shows regions where it is restricted.

directly on the stability of self-assembled structures. These results stand in comparison with those obtained for cyclic glycolipids.

We would like to thank the EPSRC and the co-sponsored Alliance Programme of the British Council and the Ministere des Affaires Etrangeres, Direction de la Cooperation Scientifique et Technique for financial support of this research work.

References

[1] Noller, C. R., and Rockwell, W. C., 1938, *J. Am. chem. Soc.*, **60,** 2076.
[2] Barrall, E., Grant, B., Oxsen, M., Samulski, E. T., Moews, P. C., Knox, J. R., Gaskill, R. R., and Haberfeld, J. L., 1979, *Org. Coat. Plast. Chem.*, **40,** 67.
[3] Jeffrey, G. A., and Bhattacharjee, S., 1983, *Carbohydr. Res.*, **115,** 53;
Jeffrey, G. A., 1986, *Acc. chem. Res.*, **19,** 168;
Jeffrey, G. A., and Wingert, L. M., 1992, *Liq. Cryst.*, **12,** 179, and references therein.
[4] Goodby, J. W., 1984, *Mol. Cryst. liq. Cryst.*, **110,** 205.
[5] Van Doren, H. A., and Wingert, L. M., 1991, *Mol. Cryst. liq. Cryst.*, **198,** 381;
Jeffrey, G. A., 1990, *ibid.*, **185,** 209.
[6] Gray, G. W., 1974, *Liquid Crystals and Plastic Crystals*, Vol. 1, edited by G. W. Gray and P. A. Winsor. (London: Ellis Horwood), pp. 103–152.
[7] Prade, H., Miethchen, R., and Vill, V., 1995, *J. prakt. Chem.*, **337,** 427.
[8] Vill, V., Böcker, T., Thiem, J., and Fischer, F., 1989, *Liq. Cryst.*, **6,** 349.
[9] Miethchen, R., Holz, J., Prade, H., and Lipták, A., 1992, *Tetrahedron*, **48,** 3061.
[10] Goodby, J. W., Haley, J. A., Watson, M. J., Mackenzie, G., Kelly, S. M., Letellier, P., Douillet, O., Godé, P., Goethals, G., Ronco, G., and Villa, P., *Liq. Cryst.* (to be published).
[11] Martin, P., Conan, J. Y., Harmouch, B., Postel, D., Ronco, G., Rouch, C., and Villa, P., 1994, *Chem. Lett.*, **1,** 141.
[12] Baker, B., Schaub, R., and Williams, J., 1962, *J. Am. chem. Soc.*, **77,** 7.
[13] Sowa, W., 1968, *Can. J. Chem.*, **46,** 1586.
[14] *CRC Handbook of Physics and Chemistry*, 1988, 68th edition edited by R. C. Priest, (Boca Raton: CRC Press).